SOILS AND FOUNDATIONS Vol. 47, No. 6, 1063–1073, Dec. 2007
Japanese Geotechnical Society

LARGE-SCALE PLANE STRAIN COMPRESSION TESTS ON COMPACTED GRAVEL WITH ACTIVE AND PASSIVE CONTROLS

SAJJAD MAQBOOL[i] and JUNICHI KOSEKI[i]

ABSTRACT

Large-scale plane strain compression tests were performed to study the effect of compaction on strength and deformation properties of gravel. The specimen is rectangular prismatic with dimensions of 50 cm in height and 22 cm times 25 cm in cross-section. By employing well-graded crushed sandstone called as Chiba gravel, five sets of plane strain compression tests were conducted on partially saturated specimens having dry densities in the range of 1.80–2.15 g/cm^3 that were prepared using manual or automatic compaction techniques. For each set of tests, one specimen was tested by following the conventional approach called as ''passive control'' of ε_2, while the second specimen was tested by following a new approach called as ''active control'' in which one of the two confining plates was allowed to move forward and backward for keeping the locally measured value of ε_2 almost zero. As a result, no significant effect of the active control was found on the stress-strain behavior as compared to the passive control, except for the beginning of shearing. The maximum deviator stresses in the two kinds of plane strain compression tests were about 20% larger than those in the relevant triaxial compression tests under the employed range of the compaction levels.

Key words: active control, compaction, deformation, gravel, plane strain compression tests, strength (**IGC**: D6)

INTRODUCTION

Compaction consists of closely packing the soil particles together by mechanical means, thus increasing the soil dry unit weight. The mechanical improvement of ground through compaction is a cost effective alternative to many stabilization techniques and involves densification of soil by applying mechanical energy. Compacted gravel has been the major constituents for the construction of huge embankments for dams, roads, railway tracks and airports.

In order to model, for example, the behavior of long embankments for roads or railways where the strain parallel to the longitudinal axis of the embankment is almost zero, plane strain compression tests are essential. Therefore, a large number of experimental studies were conducted to reveal the behavior of sandy soils under plane strain conditions (e.g., Cornforth, 1964; Marachi et al., 1969; Lee, 1970; Green and Reades, 1975; Oda et al., 1978; Tatsuoka et al., 1986; Lam and Tatsuoka, 1988; Drescher et al., 1990; Finno et al, 1997; Yoshida and Tatsuoka, 1997; Rechenmacher and Finno, 2004; Wanatowski and Chu, 2006 among others). In addition, after enlarging the scale of the test apparatus, some plane strain compression tests were also conducted on gravelly soils (e.g., Dong and Nakamura, 1997; Okuyama et al., 2003 among others). It should be noted that, in the tests conducted in these previous studies, two lateral sides of a rectangular prismatic specimen were kept fixed, using two confining plates, while the major principal stress was increased under constant confining pressure ($=\sigma_3$) until complete failure of the specimen. This method is herein named as ''passive control'' plane strain test. In these tests, fixed confining plates were employed to resist against the expansion of specimen in the intermediate principal strain ε_2 direction. Under the above conditions, however, the specimen may undergo local deformation in the ε_2 direction, due to the effect of bedding error at the interfaces between the specimen and the confining plates. Such effect would be more pronounced in testing on gravelly soils with larger grain sizes.

In the present study, therefore, in addition to the passive control tests, one of the two specimens prepared by compacting gravel under similar conditions, was tested by following a newly developed approach of plane strain compression testing, in which one confining plate was allowed to move forward and backward resulting external $\varepsilon_2 \neq 0$ while keeping the average values of ε_2 measured locally at the middle height of the specimen on two opposite sides within a range of $\pm 0.01\%$. This method is herein named as ''active control'' plane strain test, and the test results were compared with those from the passive control plane strain test and triaxial test.

[i] Associate Professor, Department of Transportation Engineering and Management, University of Engineering and Technology, Lahore, Pakistan.
[ii] Professor, Institute of Industrial Science, The University of Tokyo, Japan (koseki@iis.u-tokyo.ac.jp).
The manuscript for this paper was received for review on December 19, 2006; approved on July 18, 2007.
Written discussions on this paper should be submitted before July 1, 2008 to the Japanese Geotechnical Society, 4-38-2, Sengoku, Bunkyo-ku, Tokyo 112-0011, Japan. Upon request the closing date may be extended one month.

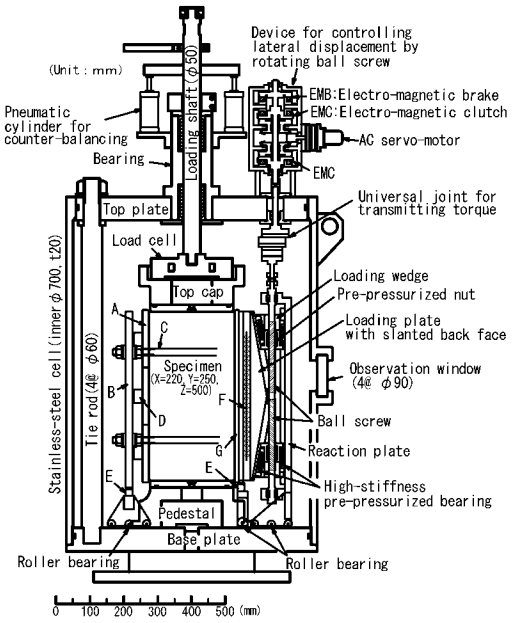

A: Confining plate (three pieces on measuring side)
B: Reaction plate
C: Tie rod connecting reaction plates (4 @ φ 20 mm)
D: Load cell to measure σ_2
E: Load cell to measure friction between specimen and confining plate
F: Cross-roller bearing
G: Confining plate (one piece on loading side)

Fig. 1. Schematic diagram of large-scale true triaxial apparatus (AnhDan et al., 2006a)

LARGE SCALE TRUE TRIAXIAL APPARATUS

A large-scale true triaxial apparatus (AnhDan et al., 2006a) was employed to conduct plane strain compression tests on gravel. This apparatus (Fig. 1) consists of a triaxial cell, axial and lateral loading devices, and a cell pressure-control device. The definition of three coordinates is presented in Photo 1. The major principal stress σ_1, is applied in the vertical (axial) direction; the intermediate principal stress σ_2 is applied in the horizontal (lateral) direction using the lateral loading device, and the minor principal stress σ_3 is applied in the other horizontal direction through the cell pressure.

The pressure cell and the top and bottom plates of the triaxial cell are made of stainless-steel. The triaxial cell has a capacity of 1 MPa for the cell pressure and 490 kN for the axial load. Four observation windows were installed on the pressure cell. The specimen is prismatic, 220 mm in width, 250 mm in length and 500 mm in height.

The axial loading device employs an electro-hydraulic actuator, having a capacity of 490 kN with a stroke of 200 mm. The axial displacement of the piston of the actuator is precisely controlled by using a device called "zero-balance system" (Hayano et al., 1999). The zero-balance system is driven by an AC servo-motor, which is connected to a series of reduction gears, electro-magnetic brakes and clutches (Santucci de Magistris et al., 1999), and it can control the vertical position of a target with a resolution of 60 μm or less. In strain-controlled tests, a small-range displacement transducer having a stroke of ± 3 mm detects the location of the loading shaft relative to the target, and a feedback is applied to the electro hydraulic actuator through a digital-servo control unit in such a way that the loading shaft smoothly follows the vertical displacement of the target.

The lateral stress σ_2 is applied by using a pair of confining plates sandwiching the specimen. The capacity, stroke, and the range of controllable strain rate of the lateral loading device are 98 kN, 20 mm, and 0.0001/m to 0.1%/m, respectively. As shown in Fig. 1, a single confining plate on the loading side (denoted as *G* in Fig. 1) is supported by a combination of a cross-roller bearing (*F*), a loading plate with slanted back face, two loading wedges, and a reaction plate. By rotating a ball screw with a motor-driven system, the two loading wedges are moved vertically in the direction opposite to each other. Vertical displacement is converted into horizontal displacement through the sliding movement along the slanted back face of the loading plate. The motor-driven system is similar to the above-mentioned device for controlling the target vertical displacement. The other confining plate (A) on the measuring side consists of three platens located at the upper-, middle-, and lower-third heights of the specimen. The platens are attached to independent load cells (D) that are fixed to the other reaction plate (B).

The reaction plates on both sides are tightly connected to each other by using four tie rods (C). The reaction plates are mounted on roller bearings placed on the base of the cell to allow possible horizontal displacements of the specimen. In order to accommodate such horizontal displacements, a universal joint is employed to connect the ball screw to control system outside the cell. Vertical friction forces between the specimen and the confining plates are measured with two load cells (E) attached to the bottom of each confining plate.

To measure the lateral force, three load cells (D) were set at the confining plate on the measuring side. Each of these load cells has a capacity of 58.8 kN.

To ensure free horizontal and vertical movements of the confining plates, the width of the cap and pedestal (in the direction perpendicular to the confining plate) is 4 mm smaller than the specimen width. When setting the confining platens on the lateral surfaces of the specimen, a horizontal gap of 2 mm was left between the lateral plates and the top cap or pedestal for each side. It is considered that the stress and strain distributions are not affected significantly by these gaps in the present study, since the grain size of the tested gravel ($D_{max} = 38$ mm and $D_{50} = 11$ mm, Fig. 4) was much larger than this gap.

As shown in Photo 1, in the case of passive control tests, axial strain (ε_1) was measured with three pairs of vertical local deformation transducers (V-LDTs) (Goto et al., 1991) in addition to external measurement with a linear variable differential transducer (LVDT). In both active and passive control tests, one of the two lateral strains (ε_2) was measured by another three pairs of horizontal local deformation transducers (H-LDTs). In

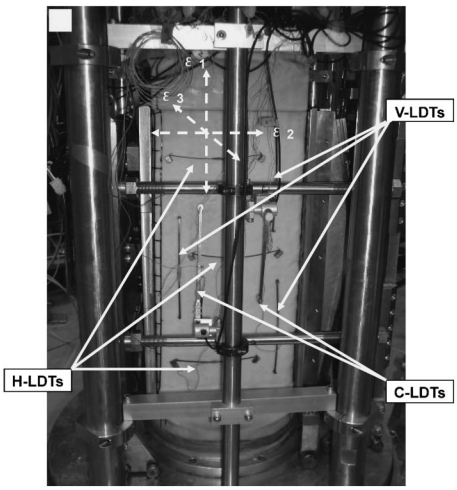

Photo 1. Prismatic specimen after setting confining plates and all types of LDTs

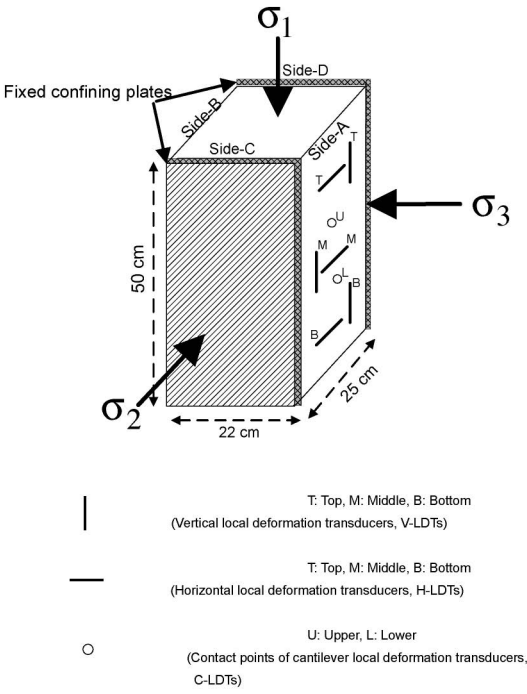

Fig. 2. Positioning of LDTs on passive control plane strain compression test specimen

order not to interfere with H-LDTs that are employed for the active control, V-LDTs were not set in the case of active control plane strain compression tests. To measure the value of second lateral strain (ε_3), a special type of deformation transducers which had been modified into a cantilever type from the original type of LDTs were used, and called hereafter as C-LDTs (refer to AnhDan et al., 2006b for the details of these new type LDTs). These were set at two different heights. The directions of ε_1, ε_2 and ε_3 are also shown in Photo 1. The LDTs are free from the effects of membrane penetration. The photo of the test specimen after setting all three types of LDTs is shown in Photo 1. The schematic diagrams showing the location of

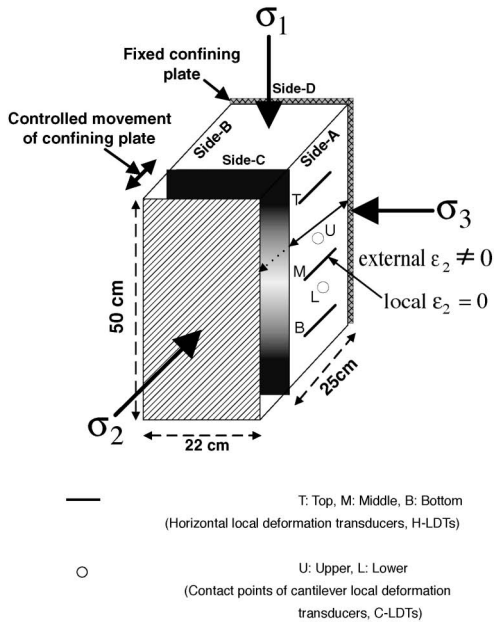

Fig. 3. Positioning of LDTs on active control plane strain compression test specimen

all LDTs over the specimen for passive and active control tests are shown in Figs. 2 and 3, respectively. The potential non-uniformity of the specimen can be evaluated by measuring local strains at three different heights, which will be reported elsewhere. To reduce the effects of friction developing between the specimen and the confining plates, top cap, and pedestal, a lubrication layer using a 200 μm-thick grease layer (commercially available as EM-30L Grease from Dow Corning Toray Silicone, Japan) and a 0.8 mm-thick membrane was inserted in between. The configuration of the lubrication layer was determined based on the results from a series of direct shear tests performed on the gravel following the procedures employed by Tatsuoka and Haibara (1985).

In the present study, while analyzing the test results, for each direction of the local strain measurement, the mean of the data measured with all two or three pairs of transducers set in the respective direction was used.

TESTED MATERIAL AND TESTING PROGRAM

The test material was a well-graded crushed sandstone having $U_c = 30$ and $\rho_s = 2.71$ g/cm^3 (called Chiba gravel) (Maqbool, 2005). It could be categorized into well-graded sandy gravel. The gradation chart of the tested material is given in Fig. 4. Specimens were prepared with varying dry density while keeping the same values of initial moisture content, as will be described later.

Throughout the tests, the backpressure was set equal to the atmospheric pressure. All the specimens were first subjected to isotropic consolidation (denoted as I.C. in the relevant figures) from a stress state of 49 kPa up to 98 kPa (stress path 1 in Fig. 5). It was followed by isotropic unloading from a stress state of 98 kPa down to 49 kPa (stress path 2 in Fig. 5). After isotropic consolidation

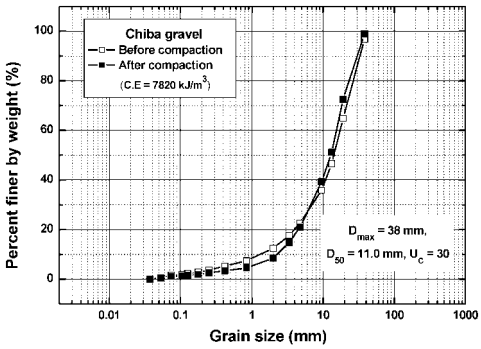

Fig. 4. Gradation curve of tested material

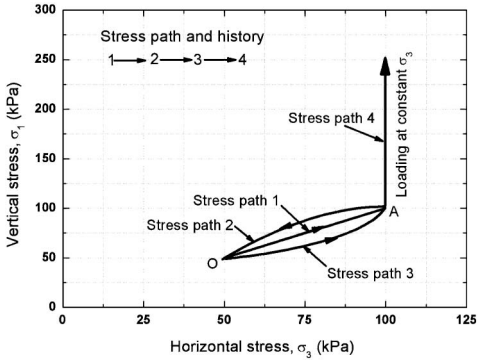

Fig. 5. Stress path employed

with small cyclic loading at several stress levels, the specimens were again subjected to isotropic consolidation from stress level of 49 kPa to 98 kPa without applying any small cycles of loading (stress path 3 in Fig. 5). These stress histories were applied without attaching the confining plates. Then, after attaching the confining plates, drained plane strain compression (denoted as P.S.C.) in the vertical direction was conducted at $\sigma_3 = 98$ kPa (stress path 4 in Fig. 5).

TEST RESULTS AND DISCUSSIONS

Preparation of Compacted Specimen

A large compaction mould (Photo 2) with inner dimensions of 25.4 cm × 22.4 cm in cross-section and 49.8 cm in height was framed to prepare compacted gravel specimen of the required size. The frame of the mould consisted of four plates fixed together with the help of screws. Moreover, lateral bracing was provided at mid-height of the mould to provide additional strength against lateral spreading of compacted material during heavy compaction. The mould was fixed over the pedestal of the cell therefore after preparation of specimen there was no need to move the specimen; rather the mould could be detached by unscrewing the bolts of four plates.

Table 1 summarizes the test conditions for each specimen employed for the present study. It should be noted that the dry density of the specimen is defined herein as the value computed based on the dry mass of the compacted material, the specimen height that was measured immediately after compaction without applying any confining stress, and the inner dimensions of the mould that was corrected for the thickness of the rubber membrane (= 2 mm).

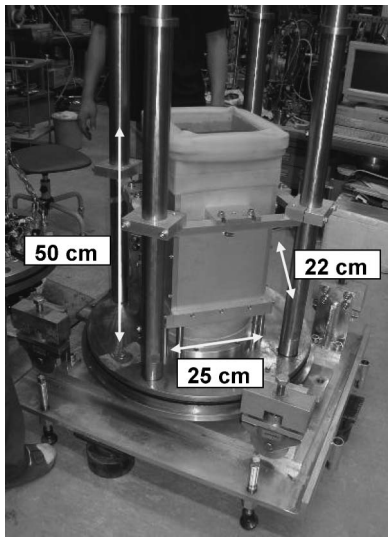

Photo 2. Large-size compaction mould to prepare gravel specimens

Table 1. Test conditions and results of plane strain tests

Set No.	Passive/ Active control test	Test Code	Compaction Energy kJ/m³	Dry density g/cm³	q_{max} kPa	Compaction by manual/ pressure/ auto
1	Passive	PS_P-1	—	1.80	373	pressure
	Active	PS_A-1	—	1.80	460	pressure
2	Passive	PS_P-2	—	1.90	630	pressure
	Active	PS_A-2	—	1.90	595	pressure
3	Passive	PS_P-3	680	1.93	660	manual
	Active	PS_A-3	680	1.93	670	manual
4	Passive	PS_P-4	6200	2.07	1160	manual
	Active	PS_A-4	6200	2.07	1139	manual
5	Passive	PS_P-5	2700	2.02	837	auto
6	Passive	PS_P-6	8685	2.15	1320	auto

PS_P: Passive control plane strain test.
PS_A: Active control plane strain test.
All the tests were conducted at $\sigma_3 = 98$ kPa.

In the first two sets of specimens as listed in Table 1, a new type of automatic compactor as shown in Photo 3, was employed as an effort to obtain higher and more uniform dry density of the specimen throughout the depth. This compactor consisted of a pneumatic cylinder, a frame for supporting the cylinder on the vertical columns of the cell as shown in Photo 3(a), a vibrator with eccentric loading motor (Photo 3(b)), different sets of springs (Photo 3(c)) with each set consisting of four springs, spacer, and a rectangular steel plate. For the

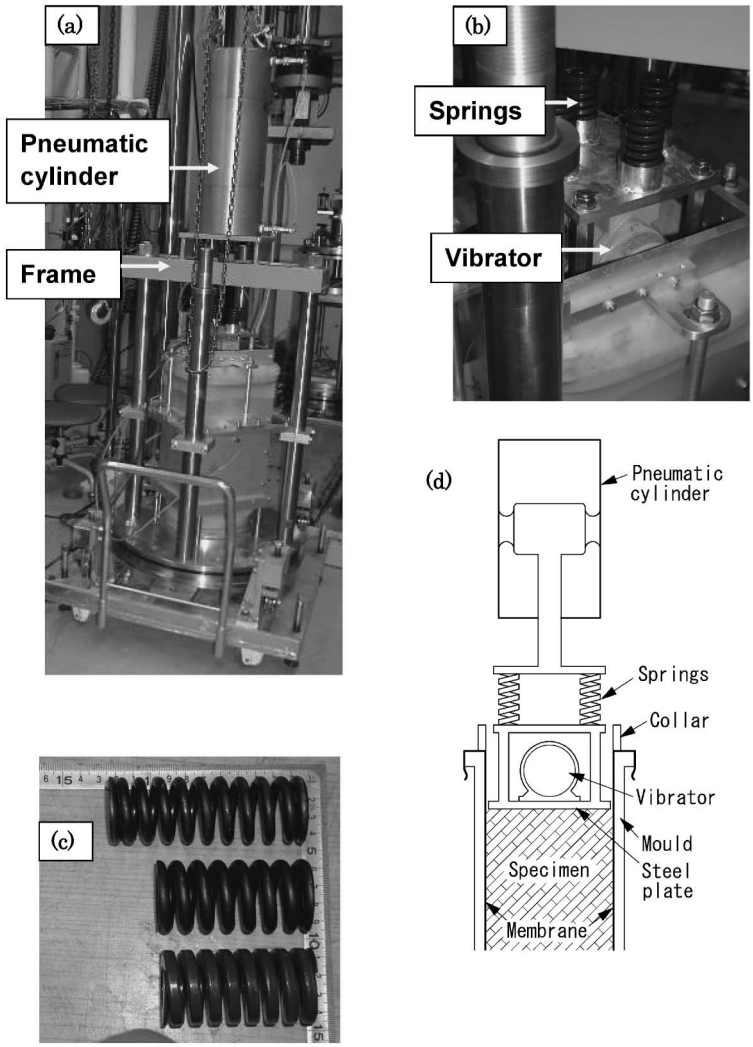

Photo 3. (a) Automatic compactor using static pressure followed by vibration, (b) Vibrator set on specimen, (c) Three different types of springs used in compactor and (d) Schematic diagram

compaction purpose, a required input stress was calculated by considering the area of the plate (21 × 24 cm) in contact with the specimen top surface inside the mould. The static stress was applied using pressurized air. Two types of loading, static and dynamic were used to apply required stress. First, static load of about 100 kPa was applied and the thickness of the layer was measured. Then by providing power supply to the motor, vibratory (dynamic) loading was applied for 5 min for each step of static loading on each layer.

For the next two sets, sets-3 and 4 (Table 1) of specimens, compaction was done by using a hammer of 12 kg mass with a fall height of 48.5 cm that was lifted by ''manual'' effort using a rope passing over a pulley or by ''automatic'' i.e., motor driven system as shown in Figs. 4 and 5. The difficulty in employing manual technique was just a need of large manual effort; otherwise reproducibility was similar to that in automatic technique (Maqbool et al., 2007).

Lastly, to prepare specimens of set-5 listed in Table 1, the ''automatic'' technique of compaction was employed in which not only the mass was lifted and dropped automatically but also the blows were counted automatically by using a counter as shown in Fig. 5(a).

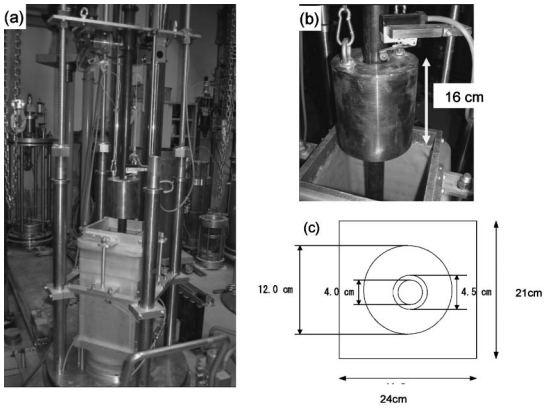

Photo 4. (a) Compactor fixed over the mould (b) Hammer having mass of 12 kg used for compaction and (c) Schematic diagram for the plan view of hammer

The compaction by any of the above techniques was performed in 11–12 layers with a compacted thickness of

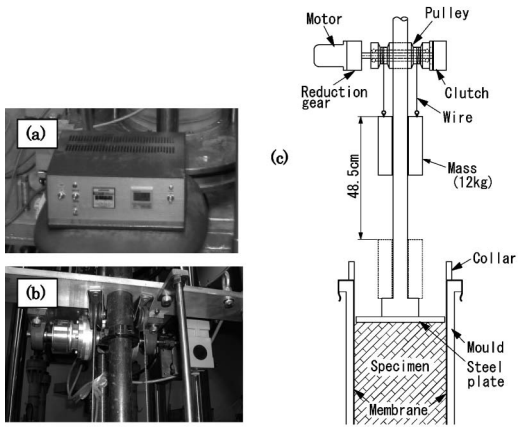

Photo 5. (a) Counter used to count number of blows, (b) Pulley, motor and clutch system to lift the hammer for free falls and (c) Schematic diagram

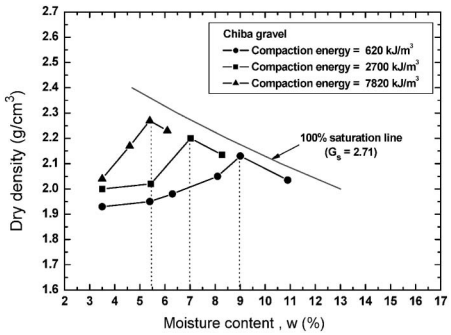

Fig. 6. Compaction curves of tested material

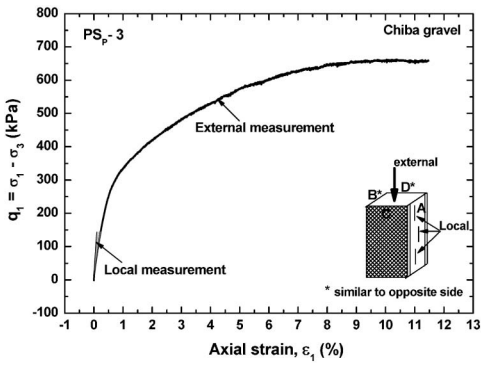

Fig. 7. Axial strain measured externally and locally versus deviator stress q_1

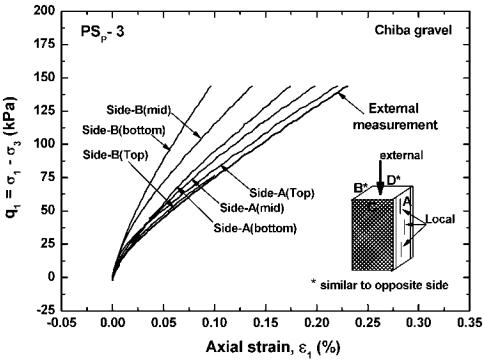

Fig. 8. Axial strain measured externally and locally versus deviator stress q_1 for initial shearing

4–4.5 cm per layer. Before placing the material for the next layer, the surface of the compacted preceding layer was scrapped to a small depth to ensure a good interlocking between vertically adjacent layers. During this study, particle breakage by heavy compaction was also checked and it was found insignificant as typically shown in Fig. 4. The dry density of the heavily compacted specimens was close to typical field values (Kohata et al., 1994). To obtain the optimum moisture content, before preparing the actual specimens, compaction curves were drawn for three levels of compaction energy i.e., 620, 2700 and 7820 kJ/m^3 and are shown in Fig. 6.

It was found that the values of the optimum moisture content were different for each level of compaction. Therefore, in order to keep consistency, the optimum moisture content obtained for the maximum level of compaction (=5.5%) was employed for all compaction levels to prepare the test specimens in this study.

Passive Control Plane Strain Compression Tests

Plane strain compression tests are necessary to model, for example, the behavior of long embankments for roads or railways where the strain parallel to the longitudinal axis of the embankment is almost zero. Therefore, in passive control plane strain compression tests, two lateral sides of the rectangular prismatic specimen are kept fixed, using two confining plates, while the major principal stress is increased under constant confining pressure ($=\sigma_3$) until complete failure of the specimen. In these conventional plane strain compression tests, as mentioned in the INTRODUCTION, fixed confining plates are employed to resist against the expansion of specimen in the intermediate principal strain ε_2 direction. Under these conditions it is assumed that just by fixing the confining plates, the intermediate principal strain ε_2 is kept at zero.

In this study, to check the effect of compaction on strength and deformation properties under plane strain condition, four specimens (Table 1) were tested following passive control testing procedure.

In these tests, the first objective was to verify the effect of bedding error caused between the side surfaces of the specimen and confining plates. Such effect of bedding error in the ε_1 direction has been already reported by a number of researchers (e.g., Tatsuoka and Kohata, 1994) and it was also confirmed in this study as shown in Figs. 7 and 8. Axial strain, ε_1 measured by the vertical LDTs showed smaller values as compared to that by external measurement (Fig. 8).

It was found that similar to the trend in ε_1 direction, intermediate principle strain ε_2 measured locally by three pairs of horizontal local deformation transducers (H-LDTs) reached 1.76% in loose specimen (Fig. 9) and ex-

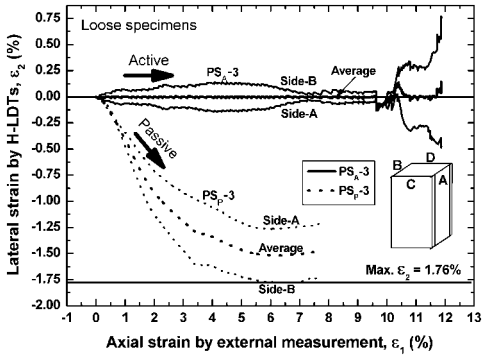

Fig. 9. Externally measured axial strain versus local intermediate principle strain in loose set of specimens

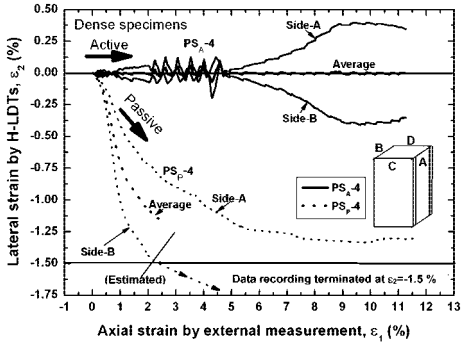

Fig. 10. Externally measured axial strain versus local intermediate principle strain in dense set of specimens

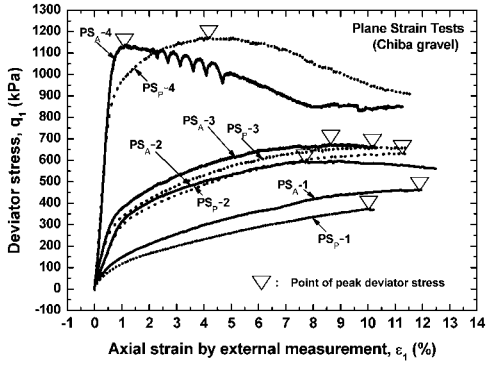

Fig. 11. Externally measured axial strain versus deviator stress q_1 in both active and passive control tests

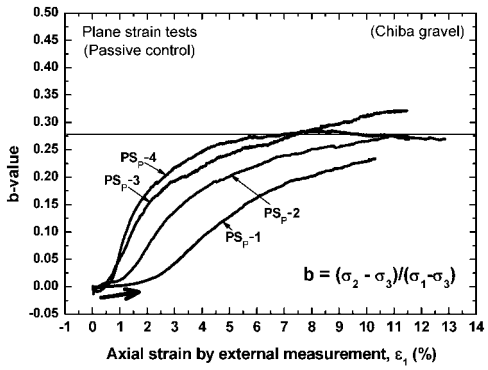

Fig. 12. Externally measured axial strain versus b-value in passive control tests

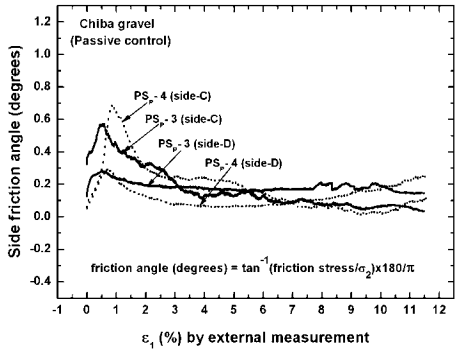

Fig. 13. Externally measured axial strain versus side friction angle in passive control tests

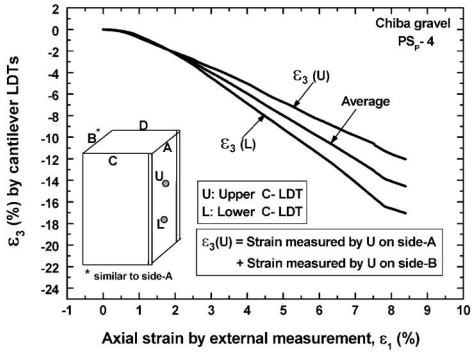

Fig. 14. Externally measured axial strain versus minor principle strain ε_3

ceeded 1.50% in dense specimen (Fig. 10). Such measurement on side-B of specimen PS_P-4 was terminated at this value due to over-scaling otherwise actual values of ε_2 could be even larger than 1.50% as shown by arrows in Fig. 10. With this specimen, larger values of ε_2 on side-B as compared to those on side-A were observed. It is possibly affected by the extents of bedding error at the interfaces between the specimen and the confining plates that might have been different from each other due to the heterogeneity of the well-graded specimen.

The stress-strain relationship for all four specimens during plane strain compression is shown in Fig. 11. The specimens with higher density, showed higher peak deviator stress. In terms of b-value ($=(\sigma_2-\sigma_3)/(\sigma_1-\sigma_3)$) in all four specimens gradual increase was observed in the beginning of shearing as shown in Fig. 12. The values of side friction angle measured with two friction load cells were found negligible in all tests as shown in Fig. 13.

The average magnitude of minor principle strain ε_3 reached to a level of about 16% at the axial strain ε_1 of about 8% as shown in Fig. 14. Nominal volumetric strain was measured by Eq. (1).

$$\varepsilon_{vol} = \varepsilon_1 + \varepsilon_3 \tag{1}$$

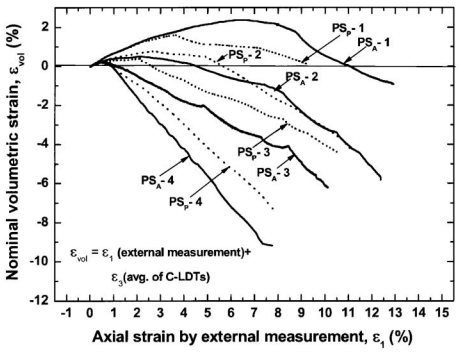

Fig. 15. Externally measured axial strain versus nominal volumetric strain ε_{vol}

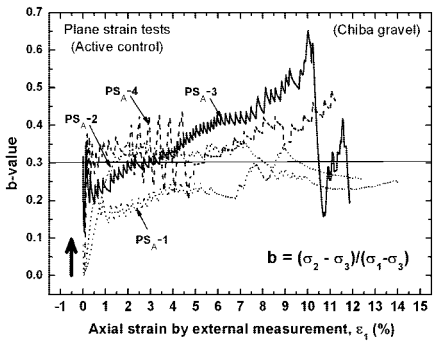

Fig. 16. Externally measured axial strain versus *b*-value in active control tests

Here ε_{vol} is the nominal volumetric strain, ε_1 is the axial strain measured externally and ε_3 is the strain measured by C-LDTs. ε_{vol} showed less dilative behavior in the case of looser specimens than those in denser specimens as shown in Fig. 15. Such difference in dilatancy curves represented the difference in compaction level or dry density for all four specimens.

It should be noted that, as typically shown in Fig. 14, the ε_3 values measured at the upper level of the specimen were not equal to those at the lower level. Such difference is possibly affected by the heterogeneity of the well-graded specimen as well.

Active Control Plane Strain Compression Tests

Four specimens as listed in Table 1 were tested by following the procedure of active control plane strain compression test.

In these tests, the average of intermediate principle strain ε_2 measured locally at the middle height of the specimen on both sides A and B, could be successfully controlled within a range of $\pm 0.01\%$ as typically shown in Figs. 9 and 10.

In contrast to the passive control tests *b*-value ($=(\sigma_2-\sigma_3)/(\sigma_1-\sigma_3)$) in all four specimens increased rapidly to a level of about 0.3 as shown in Fig. 16, which means σ_2 could be mobilized effectively even at the beginning of vertical loading.

For the stress-strain relationship, the deviator stress $q_1(=\sigma_1-\sigma_3)$ was plotted against axial strain (ε_1) for all four specimens of active control tests compacted at different compaction energies as shown in Fig. 11. It was observed that q_1 values at the same axial strain were larger in denser specimens than those in relatively loose specimens.

Moreover, it was found that for similar density the maximum deviator stress (q_{max}) corresponding to peak deviator stress in active control tests was not largely different from that of passive control tests. The only difference between the two types of tests was found in the beginning of shearing for all four sets of specimens as shown in Fig. 17. In conducting plane strain compression tests, therefore, such active control of confining plates would be required only when the behavior at the beginning of shearing is concerned. On the other hand, passive

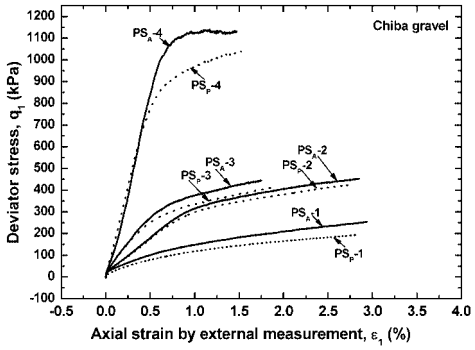

Fig. 17. Externally measured axial strain versus deviator stress q_1 for the beginning of shearing

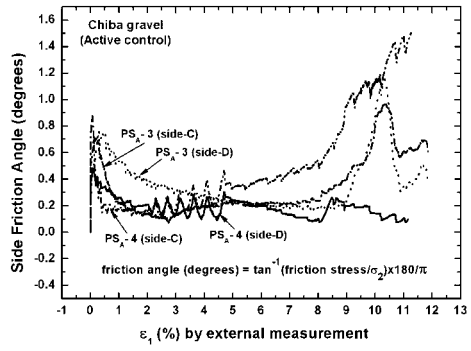

Fig. 18. Externally measured axial strain versus side friction angle in active control tests

control of confining plates would be sufficient in studying the large strain behavior, including the peak strength characteristics.

In the case of the active control tests, the side friction angle was found to increase at large axial strain levels as typically shown in Fig. 18, due possibly to the effects of formation of shear band in the specimen. If the shear band is formed in a direction that is not perfectly perpendicular to the confining plates, shear displacement along the shear band would cause uneven contact between the specimen and the confining plates, resulting into mobilization of larger friction angle.

The values of ε_{vol} measured in active control tests

showed less dilative behavior than those in passive control tests in the case of looser specimens, while this trend was opposite in dense specimens as shown in Fig. 15.

Strength Ccharacteristics of Active and Passive Control Plane Strain Compression Tests

The strength of specimen can be represented either by the maximum deviator stress (q_{max}) or by the peak angle of internal friction (ϕ_{max}) that was computed from the values of major principle stress σ_1 and the confining stress σ_3 by assuming no cohesion as:

$$\phi_{max} = \sin^{-1}[(\sigma_1 - \sigma_3)/(\sigma_1 + \sigma_3)] \quad (2)$$

It should be noted that the same definition of the peak angle of internal friction as above has been adopted in the evaluation of seismic active earth pressure for ductility design of abutment foundations for highway bridges in Japan (Shirato et al., 2006).

Note also that the Mohr-Coulomb failure criterion assumes that the ϕ_{max} values are independent of the levels of the intermediate principal stress, while there are other failure criterions that can reflect the effects of the intermediate principal stress on the strength properties. Since the Mohr-Coulomb failure criterion is most frequently employed in practice, such as stability analyses, evaluation of earth pressures and bearing capacities, comparisons were made in the latter part of this section between the results from plane strain compression tests conducted in the present study and those from relevant triaxial compression tests in terms of ϕ_{max} values as well as q_{max} values. Such information would be useful in converting the strengths obtained by conventional triaxial tests into those under plane strain condition.

To see the trend of change in q_{max} values with respect to change in dry density, only q_{max} values from Fig. 11 were taken and these are plotted in Fig. 19. It was found that q_{max} versus dry density relationship was non-linear as approximated by the polynomial equation shown in the figure.

In the second part of comparison, ϕ_{max} values were plotted against dry density as shown in Fig. 20. After such conversion, the relationship between ϕ_{max} and dry density became more linear as approximated by the equation shown in the figure.

To obtain a relationship between compaction energy and q_{max} values, two additional passive control plane strain compression tests (Sets-5 and 6) were conducted as given in Table 1. The results are shown in Fig. 21. The trend of line between q_{max} and compaction energy was found non-linear as approximated by the equation shown in the figure.

For comparison, results from a series of triaxial compression tests on the same material (Maqbool et al., 2007) are also shown in Fig. 21. The testing conditions of the triaxial compression tests are given in Table 2. The specimens for the triaxial compression tests were prepared by compacting the material in a mould employing the same procedures as for the present study, and they were sheared under drained condition without using the confining plates at the same axial strain rate as employed for the present study. It was found that the difference in the absolute values of q_{max} between the plane strain and the triaxial compression tests increased with the compaction level of the specimens.

It would be worth mentioning that specimen for PS_P-5 was prepared by employing compaction energy of 2700 kJ/m^3 which is the maximum level of compaction recommended by ASTM D1557–00 to obtain compaction curves.

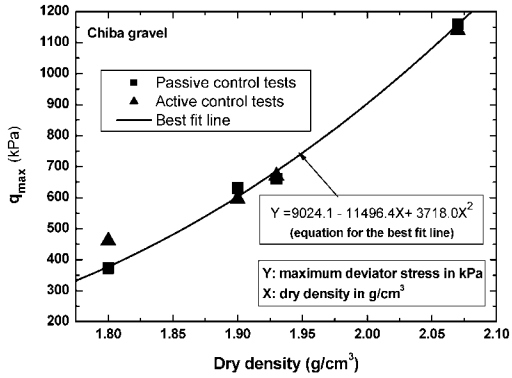

Fig. 19. Dry density versus maximum deviator stress in active and passive control tests

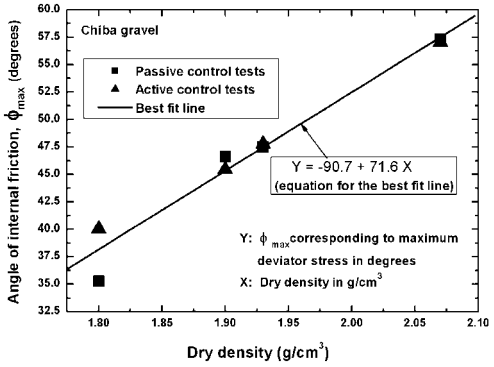

Fig. 20. Dry density versus angle of internal friction in active and passive control tests

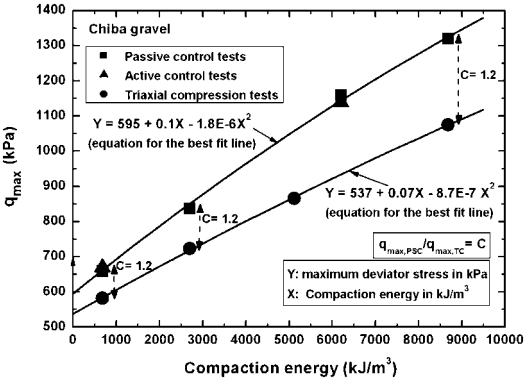

Fig. 21. Compaction energy versus maximum deviator stress in plane strain and triaxial compression tests

Table 2. Test conditions and results of triaxial tests (Maqbool et al., 2007)

Specimen no	Test code	Compaction energy (kJ/m^3)	Dry density (g/cm^3)	q_{max} (kPa)	Manual/auto compaction
1	TC-1	680	1.92	582	manual
2	TC-15	2700	2.01	723	auto
3	TC-16	5120	2.06	866	auto
4	TC-11	8685	2.17	1075	auto

TC: Triaxial compression test
All the tests were conducted at $\sigma_3 = 98$ kPa.

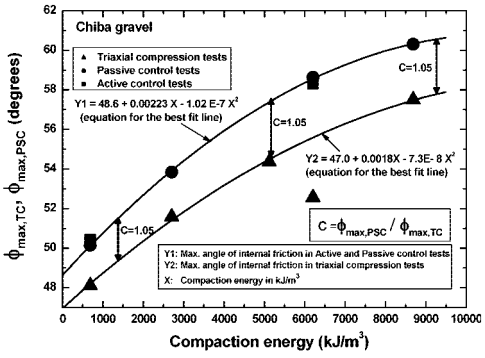

Fig. 22. Compaction energy versus angle of internal friction in plane strain and triaxial compression tests

In Fig. 21 the ratio of $q_{max,\,PSC}/q_{max,\,TC}$ is indicated at three compaction levels. The peak deviator stress q_{max} in the two kinds of plane strain compression tests were about 20% larger than that in the triaxial compression tests irrespective of the different compaction levels. Since large-scale plane strain compression apparatuses are not widely available, such empirical ratio between the peak deviator stresses may be used in estimating the peak strength under plane strain condition based on the triaxial compression test results on compacted gravels.

In order to compare the peak strengths in terms of the ϕ_{max} values between plane strain and triaxial compression tests, they are plotted against the compaction energy in Fig. 22. As a result, the ratio of $\phi_{max,\,PSC}/\phi_{max,\,TC}$ was found to be about 1.05 irrespective of the compaction levels. In other words, the difference between $\phi_{max,\,PSC}$ and $\phi_{max,\,TC}$ was about 2 degrees at low compaction levels, while it increased slightly up to about 3 degrees at high compaction levels. Such difference in the ϕ_{max} values between plane strain and triaxial compression tests on compacted gravel is consistent with those on medium-dense sands as reported by Cornforth (1964), Marachi et al. (1969), and Green and Reades (1975), while much larger difference was reported by Tatsuoka et al. (1986), and Wanatowski and Chu (2006). Future studies are required on possible effects of soil gradation, particle shape, dilatancy property and/or confining pressure on these differences.

It should be noted that, as reported by Lam and Tatsuoka (1988), the difference in the strengths under plane strain and triaxial compression conditions is affected by anisotropy or the directions of principal stresses with respect to the material axes. In the present study, on the other hand, the direction of the major principal stress was fixed to be normal to the bedding plane. It is, therefore, required to consider such effect of anisotropy in converting the strengths under triaxial compression condition into those under plane strain condition for more general stress states with the direction of the major principal stress that is deviated from the normal direction to the bedding plane. Future studies are required to clarify this issue.

CONCLUSIONS

The results from the present study can be summarized as follows.

1. Under the plane strain test conditions employed in the present study, no significant effect of the active control of ε_2 was found on the stress-strain behavior except at the beginning of shearing.
2 The difference in the absolute values of the peak deviator stresses q_{max} between the plane strain and the triaxial compression tests increased with the compaction level of the specimens, while the q_{max} values in the two kinds of plane strain compression tests were about 20% larger than those in the triaxial compression tests under the employed range of the compaction levels.

ACKNOWLEDGEMENT

The authors would like to thank Mr. Takeshi Sato, Research Support Promotion Member, Institute of Industrial Science, the University of Tokyo, for providing technical support in conducting experiments at IIS. Thanks also go to the Ministry of Science, Culture and Education of Japan for its financial support to the first author for his PhD studies at the University of Tokyo, Japan.

REFERENCES

1) AnhDan, L. Q., Koseki, J. and Sato, T. (2006a): Evaluation of quasi-elastic properties of gravel using a large-scale true triaxial apparatus, *Geotechnical Testing Journal*, ASTM, **29**(5), 374–384.
2) AnhDan, L. Q., Tatuoka, F. and Koseki, J. (2006b): Viscous effects on the stress-strain behavior of gravelly soil in drained triaxial compression, *Geotechnical Testing Journal*, ASTM, **29**(4), 330–340.
3) ASTM D1557–00: Standard test methods for laboratory compaction characteristics of soil using modified effort (2700 kN-m/m^3).
4) Cornforth, D. H. (1964): Some experiments on the influence of strain conditions on the strength of sand, *Geotechnique*, **14**(2), 143–167.
5) Dong, J. and Nakamura, K. (1997): Anisotropic deformation and strength characteristics of gravels in large-scale plane strain and triaxial compression tests, *Proc. 14th ICSMFE*, Hamburg, Germany, **1**, 81–84.
6) Drescher, A., Vardoulakis, I. and Han, C. (1990): A biaxial apparatus for testing soils, *Geotechnical Testing Journal*, ASTM,

29(5), 374–384.
7) Finno, R. J., Harris, W. W., Mooney, M. A. and Viggiani, G. (1997): Shear bands in plane strain compression of loose sand, *Geotechnique*, **47**(1), 149–165.
8) Goto, S., Tatsuoka, F., Shibuya, S., Kim, Y. S. and Sato, T. (1991): A simple gauge for local small strain measurements in the laboratory, *Soils and Foundations*, **31**(1), 169–180.
9) Green, G. E. and Reades, D. W. (1975): Boundary conditions, anisotropy and sample shape effects on the stress-strain behaviour of sand in triaxial compression and plane strain, *Geotechnique*, **25**(2), 333–356.
10) Hayano, K., Koseki, J., Sato, T. and Tatsuoka, F. (1999): Small strain deformation characteristics of sedimentary soft mudstone from true triaxial tests, *Proc. Pre-failure Deformation Characteristics of Geomaterials*, Jamiolkowski, Lancellotta and Lo Presti (eds.), **1**, 191–198.
11) Kohata, Y., Tatsuoka, F., Dong, J., Teachavorasinskun, S. and Mizumoto, K. (1994): Stress states affecting elastic deformation moduli of geomaterials, *Proc. International Symposium on Prefailure Deformation of Geomaterials*, **1**, 3–10.
12) Lam, W. K. and Tatsuoka, F. (1988): Effects of initial anisotropic fabric and σ_2 on strength and deformation characteristics of sand, *Soils and Foundations*, **28**(1), 89–106.
13) Lee, K. L. (1970): Comparison of plane strain and triaxial tests on sand, *Journal of the Soil Mechanics and Foundations Division, Proc.* ASCE, **96**(SM3), 901–923.
14) Maqbool, S. (2005): Effect of compaction on strength and deformation properties of gravel in triaxial and plane strain compression tests, *PhD Thesis*, Civil Engineering Department, the University of Tokyo, Japan.
15) Maqbool, S., Koseki, J. and Sato, T. (2007): Effects of compaction on strength and deformation properties of gravel in triaxial compression tests, *Journal of Geotechnical and Geoenvironmental Engineering* ASCE, (submitted for possible publication).
16) Marachi N. D., Chan, C. K., Seed, H. B. and Duncan, J. M. (1969): Strength and deformation characteristics of rockfill materials, *Report No. TE–69–5*, Department of Civil Engineering, University of California, Berkeley, 139.
17) Oda, M., Koishikawa, I. and Higuchi, T. (1978): Experimental study of anisotropic shear strength of sand by plane strain test, *Soils and Foundations*, **18**(1), 25–38.
18) Okuyama, Y. Yoshida, T., Tatsuoka, F., Koseki, J., Uchimura, T., Sato, N. and Oie, M. (2003): Shear banding characteristics of granular materials and particle size effects on the seismic stability of earth structures, *Proc. Deformation Characteristics of Geomaterials* (eds. by Di Benedetto, Doanh, Geoffroy and Sauzeat), 607–616.
19) Rechenmacher, A. L. and Finno, R. J. (2004): Digital image correlation to evaluate shear banding in dilative sands, *Geotechnical Testing Journal*, ASTM, **27**(1), 13–22.
20) Santucci de Magistris, F., Koseki, J., Amaya, M., Hamaya, S., Sato, T. and Tatsuoka, F. (1999): A triaxial testing system to evaluate stress-strain behaviour of soils for wide range of strain and strain rate, *Geotechnical Testing Journal*, ASTM, **22**(1), 44–60.
21) Shirato, M., Fukui, J. and Koseki, J. (2006): Current status of ductility design of abutment foundations against large earthquakes, *Soils and Foundations*, **46**(3), 377–396.
22) Tatsuoka, F. and Haibara, O. (1985): Shear resistance between sand and smooth or lubricated surfaces, *Soils and Foundations*, **25**(1), 89–98.
23) Tatsuoka, F. Sakamoto, M., Kawamura, T. and Fukushima, S. (1986): Strength and deformation characteristics of sand in plane strain compression at extremely low pressures, *Soils and Foundations*, **26**(1), 65–84.
24) Tatsuoka, F. and Kohata, Y. (1994): Bedding error, *Tsuchi-to-Kiso*, JGS, **42**(9), Ser.No.440, 53–55 (in Japanese).
25) Yoshida, T. and Tatsuoka, F. (1997): Deformation property of shear band in sand subjected to plane strain compression and its relation to particle characteristics, *Proc. 14th ICSMFE*, Hamburg, **1**, 237–240.
26) Wanatowski, D. and Chu, J. (2006): Stress-strain behavior of a granular fill measured by a new plane-strain apparatus, *Geotechnical Testing Journal*, ASTM, **29**(2), 149–157.